coatings

MDPI

Article

In Silico Screening and Design of Coating Materials for PEMFC Bipolar Plates

Longjie Liu [1,2], Li Yao [3], Kai Feng [1,2,*], Zhe Luo [4], Ke Liu [4], Hong Zhu [4] and Paul. K. Chu [2]

1 Shanghai Key laboratory of Materials Laser Processing and Modification, School of Materials Science and Engineering, Shanghai Jiao Tong University, Shanghai 200240, China; llj10429@sjtu.edu.cn
2 Department of Physics and Materials Science, City University of Hong Kong, Tat Chee Avenue, Kowloon, Hong Kong, China; paul.chu@cityu.edu.hk
3 SAIC Motor Co. Ltd., Shanghai 201800, China; YaoLi01@saicmotor.com
4 University of Michigan-Shanghai Jiao Tong University Joint Institute, Shanghai 200240, China; zheluo@umd.edu (Z.L.); xxy1995@sjtu.edu.cn (K.L.); hong.zhu@sjtu.edu.cn (H.Z.)
* Correspondence: fengkai@sjtu.edu.cn; Tel.: +86-21-5474-5878; Fax: +86-21-3420-3024

Received: 18 September 2018; Accepted: 27 October 2018; Published: 29 October 2018

Abstract: Methods used to design coating materials for polymer electrolyte membrane fuel cells (PEMFCs) are unsystematic and time-consuming because current materials research relies on scientific intuition and trial and error experimentation. In this study, a feasible and more efficient scheme of screening and designing coating materials is established based on density function theory (DFT) utilizing the fast-growing computing capacity. The scheme consists of four steps: Elements selection by calculation of Pilling–Bedworth ratio and electrical resistivity, corrosion resistance assessment leveraging the Pourbaix diagram approach, running BoltzTrap code to calculate electrical conductivity (σ/τ), and interface binding strength evaluation by calculation of separation work. According to the calculation results, TiCo and $TiCo_3$ are proposed to be the two most promising candidates because of relatively better properties required by harsh working environment of PEMFC. The high-throughput screening strategy established in this study makes the ideal of rapidly evaluating hundreds of thousands of possible coating materials candidates into reality and helps to indicate the direction of further synthesis efforts.

Keywords: fuel cell; high-throughput; DFT; bipolar plates; coating materials

1. Introduction

With the increasing concern of fossil fuel reserves and environment protection, hydrogen energy has attracted much attention as well as related research. The polymer electrolyte membrane fuel cell (PEMFC), using hydrogen as the fuel, is an ideal candidate for power sources in automotive propulsion applications and power plants due to its high power density and efficiency, low working temperature, fast start-up, and near-zero emission [1–4]. However, the development of PEMFC is hindered by some issues, mainly insufficient durability and high cost [5].

As a key component of the PEMFC stack, the bipolar plate is used to support the stack, collect cell current, manage exhaust heat and water, and separate individual cells [6–8]. Because of the functional requests listed above and the harsh working environment, an effective bipolar plate should have high corrosion resistance, low interfacial contact resistance (ICR), and low cost [9]. Stainless steel is now considered a suitable material for bipolar plates since it possesses most of the properties required. However, surface modification is still necessary since it lacks the ability to combat corrosion in an acidic environment for adequate working hours [10,11]. Therefore, investigations of cost-efficient coatings which improve corrosion resistance and electrical conductivity, as well as coating materials design methods, are crucial to enhance cell performance.

The development of coating materials started from elementary substances like graphene to transition metal nitrides and carbides, and now, to element/compound multilayers to eliminate defects such as pinholes [12–14]. Until now, methods used in the design of coating materials are unsystematic and time-consuming because current materials research relies on scientific intuition and trial and error experimentation [15]. Thus, a systematic and more efficient method is needed to help researchers jump out of the repetitive "experiment and characterization loop". With the rapid development in computing capacity, computational screening and analysis makes this possible. During the past few decades, in silico screening and design of functional materials based on electronic structure calculations and structural simulation tools has accelerated the pace of materials design by rapidly evaluating hundreds and thousands of possible candidates. Greeley et al. [16] identified a new electrocatalyst BiPt out of 700 binary surface alloys for the hydrogen evolution reaction through a DFT-based high-throughput screening strategy. The synthesized BiPt was tested and found to be better than the archetypical catalyst. Kirklin et al. [17] screened out $CoSi_2$, TiP, and $NiSi_2$ as three promising materials for Li-ion battery anodes by using the DFT + GCLP (grand canonical linear programming) automated tool to evaluate 515 thermodynamically stable lithiation reactions on the basis of specific criteria. Besides these, in silico screening techniques have been also applied in areas like thermal conductivity [18], drug discovery [19], and methane storage [20]. This powerful design method is now recognized to help indicate the direction of synthesis efforts. But so far, there are few works on designing coating materials for PEMFC bipolar plates with a computational method, thus, our emphasis is to establish several criteria and a corresponding screening scheme.

In this present paper, we introduce a computational screening procedure for coating materials of bipolar plates using density function theory (DFT) calculations. We established corrosion resistance criteria, detailed conductivity assessments, and a database of DFT calculations. According to the screening result, TiCo and $TiCo_3$, intermetallic compounds formed between titanium and cobalt, are the most promising candidate materials. They are calculated to have better predicted corrosion resistance, electrical conductivity, and combination between stainless steel substrates than other binary compounds. Our efforts provide a systematic and feasible way to design coating materials for PEMFC bipolar plates and we hope it could lead to the further synthesis and testing of the identified candidate materials.

2. Methods

2.1. Computational Methods

We set up a computational screening procedure to indicate the direction of experimentation; this approach is summarized in Figure 1. Beginning with all elements on the periodic table, we take electrical resistivity, the Pilling–Bedworth ratio [21], and cost into account (these data can be found and calculated from a DFT database [22]); 13 elements (Cu, Nb, Ni, Hf, Zr, V, Cr, Ti, Mo, Ta, W, Al, and Co) were chosen. These elements combine with each other to form stable intermetallic compounds (energy above hull = 0) and, together with their stable nitrides and carbides, are on our researching list. Their nitrides and carbides are included because they are reported as "metallic ceramics" with many desirable characteristics which are widely applied and investigated in current works [11]. Next, a corrosion resistance assessment of compounds from the former step was carried out by application of the Pourbaix diagram. Then, electrical conductivity was calculated using BoltzTrap code. At last, separate work between coatings and stainless steel was studied using DFT calculations. All compounds were ranked by calculated performance metrics and the most attractive candidate was shown.

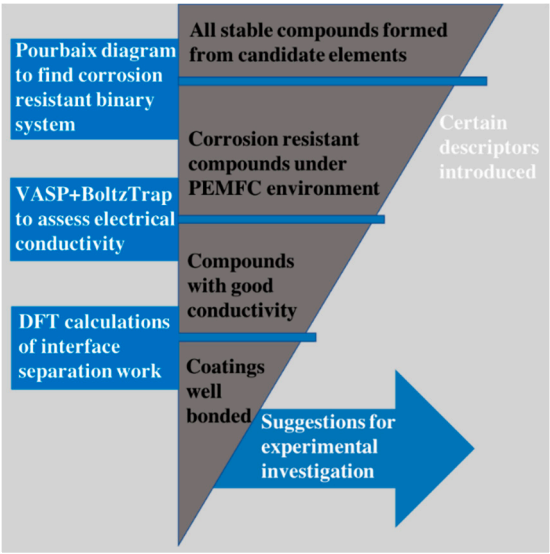

Figure 1. Process of screening to find suggestions for experimental investigation.

2.1.1. Corrosion Resistance Assessment

The corrosion resistance assessment is carried out by the use of Pourbaix diagrams (also called the electrode potential-pH diagrams). Pourbaix diagrams are maps of multidimensional thermodynamic space and areas of immunity, passivity, and corrosion [23]. Chemical and electrochemical equilibria information is reasonably summarized in the diagrams so they serve as a straightforward materials chemistry tool to learn the thermodynamics stabilities of metals in aqueous solutions [24]. This tool has been widely applied in areas of corrosion protection, inorganic chemistry, and hydrometallurgy [25] since they depict pictures of reaction products in solutions as functions of pH and potential. The Pourbaix diagram of the TiCo at 353 K (Figure 2) is constructed using first principle calculation combined with some experimental measurements [26,27]. As indicated in the diagram, the immunity domain (with only solid TiCo in it) is quite low with an equilibrium potential of dissolution of −1.9 V. With increasing electrode potential, TiCo corrodes in acid solutions and undergoes dissolution of titanium followed by cobalt. Then the passivation domain is proceeded which is mainly composed of TiO_2. The passivation film is formed on the surface of TiCo and acts as a barrier preventing TiCo from further dissolution. Bipolar plates work in an environment of pH 1–5 and electrode potential 0–1 V. The corresponding region is a passivation domain covered by solid TiO_2 and bivalent cobalt iron, which indicates a possible stable situation that maintain high corrosion resistance in acidic working environment. With the use of Pourbaix diagrams, all candidates are evaluated to screen out compounds that can exist stably or protected by dense passivation films.

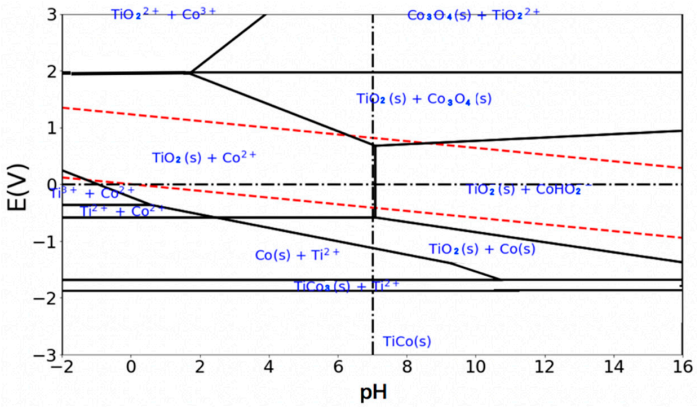

Figure 2. Pourbaix diagram of the TiCo at 353 K.

2.1.2. Electrical Conductivity Assessment

The electrical conductivity of candidate compounds has been studied using density functional and semiclassical Boltzmann transport theories. Madsen and Singh [28] established the BoltzTrap code based on Boltzmann transport theory and a well smoothed Fourier interpolation to analyze the band expression for finding thermoelectrical materials. We run the BoltzTrap code based on the DFT-calculated electronic structure under constant relaxation time approximation of the charge carriers to obtain one of the transport properties, electrical conductivity (σ/τ), which has been well tested as an accurate method to evaluate the movement of electrical charge in a substance [29–31]. Electrical conductivity tensors that are based on the rigid band approach are expressed by the following equations.

$$\sigma_{\alpha\beta}(i,k) = e^2\tau_{i,k}v_\alpha(i,k)v_\beta(i,k) \quad (1)$$

$$\sigma_{\alpha\beta}(\varepsilon) = \frac{1}{N}\sum_{i,k}\sigma_{\alpha\beta}(i,k)\frac{\delta(\varepsilon - \varepsilon_{i,k})}{\mathrm{d}(\varepsilon)} \quad (2)$$

where N is the number of k-points sampled, while the k-dependent conductivity tensor is given by Equation (1), in which τ, the relaxation time, is set to kept constant because it is direction independent after a detailed study of approximation. Electrical conductivity as a function of temperature T and chemical potential μ is given by integrating the transport distribution in Equation (3).

$$\sigma_{\alpha\beta}(T,\mu) = \frac{1}{\Omega}\int \sigma_{\alpha\beta}(\varepsilon)[-\frac{\partial f_0(T,\varepsilon,\mu)}{\partial\varepsilon}]\,\mathrm{d}\varepsilon \quad (3)$$

where α and β stand for tensor indicators. Ω, μ and f_0 are unit cell volume, carrier concentration, and Fermi–Dirac distribution function, respectively. The electrical conductivity of corrosion resistant compounds are calculated through this way.

2.1.3. Separation Work of Interface

In order to rank the stability of interfaces formed between coatings and 316 stainless steel, we carried out ab initio calculations to study atomic structures and energetics of those interfaces. The density functional theory (DFT) calculations with Perdew–Burke–Erzerhof (PBE) [32] generalized gradient approximation (GGA) and projector augmented wave (PAW) [33] pseudopotentials were performed within the Vienna Ab initio simulation package (VASP) [34]. As the interfaces contain a ferromagnetic phase, bcc Fe, a spin-polarized calculation was performed. For all configurations constructed, the plane-wave cut off energy was set to 520 eV. The k-point density of at least 1000/(numbers of atoms in unit cell) were similar to those used in the materials project (MP), which have been tested extensively over a broad range of chemistries [22].

In practical, coherent, semicoherent, or noncoherent interfaces form between bcc Fe and candidate compounds due to different lattice mismatch. But to rank the stability of interfaces for so many compounds, we simplify the atomic model as coherent interface oriented according to the so-called Baker–Nutting relation (Equation (4)), which is illustrated in Figure 3.

$$\{001\}_{\text{compounds}}\Big|\Big|\{001\}_{\text{Fe}},\ [100]_{\text{compounds}}\Big|\Big|[110]_{\text{Fe}} \quad (4)$$

The interface structure is simulated by a periodic supercell with 8 layers of bcc-Fe and 8 layers of compounds. The convergence tests for this atomic structure with respect to n_{Fe} (layers of bcc-Fe) show that n_{Fe} = 5 is already able to eliminate the interface energy error stemming from the finite size of computational unite cell [35]. So we chose n_{Fe} = 8 to fit the requirement and $n_{\text{compounds}}$ = 8 in order to produce two identical interfaces within the computational unit cell. Structural relaxation calculation was carried out with minimizing total energy. The total interface energy E_{total} is composed of two terms:

$$E_{total} = E_{chemistry} + E_{elastic} \quad (5)$$

where $E_{chemistry}$ stands for the chemistry part of total energy which stemming from breaking and forming of bonds in constructing the interface. $E_{elastic}$ is the elastic energy originating from creating the interface.

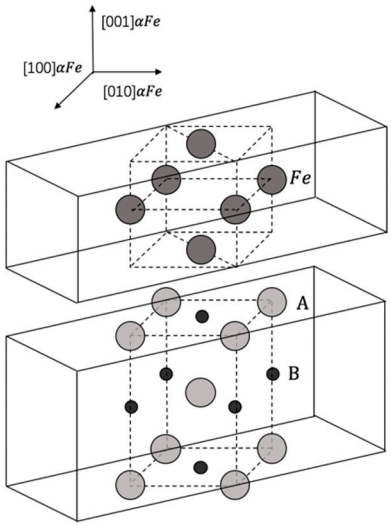

Figure 3. Schematic illustration of interface atomic configuration at Baker–Nutting orientation. *A*: larger atom in binary compound; *B*: smaller atom in binary compound.

We constructed the planar interface between two phases, Fe and the candidate compound, with different lattice spacings, $a^{(1)}$ and $a^{(2)}$. We assume $a^{(2)} > a^{(1)}$, so Fe slab is expanded while compound slab is compressed, so as to meet with the common constant $a^{(3)}$ (Equation (6)) which minimizes the elastic contribution (Equation (7)) to the total interface energy according to linear elasticity theory [36].

$$a^{(3)} = \frac{a^{(1)}a^{(2)^2}\left[C_{11}^{(1)} + C_{12}^{(2)} - 2\frac{C_{12}^{(1)^2}}{C_{11}^{(1)}}\right] + a^{(1)^2}a^{(2)}\left[C_{11}^{(2)} + C_{12}^{(2)} - 2\frac{C_{12}^{(2)^2}}{C_{11}^{(2)}}\right]}{a^{(2)^2}\left(C_{11}^{(1)} + C_{12}^{(1)} - 2\frac{C_{12}^{(1)2}}{C_{11}^{1}}\right) + a^{(1)2}\left(C_{11}^{(2)} + C_{12}^{(2)} - 2\frac{C_{12}^{(2)^2}}{C_{11}^{(2)}}\right)} \tag{6}$$

$$E_{elastic} = \epsilon_{||}^{(1)^2}\left(C_{11}^{(1)} + C_{12}^{(1)} - 2\frac{C_{12}^{(1)^2}}{C_{11}^{(1)}}\right) + \epsilon_{||}^{(2)^2}\left(C_{11}^{(2)} + C_{12}^{(2)} - 2\frac{C_{12}^{(2)^2}}{C_{11}^{(2)}}\right) \tag{7}$$

where C_{11} and C_{12} are the elastic constants and $\epsilon_{||}$ is strain parallel to the interface plane given by

$$\epsilon_{||}^{(1)} = \frac{a^{(2)} - a^{(1)}}{a^{(1)}} \tag{8}$$

The parallel strain to the interface is always accompanied by strain perpendicular to the interface (Poisson effect) given as

$$\epsilon_{\perp}^{(1)} = -2\frac{C_{12}^{(1)}}{C_{11}^{(1)}}\epsilon_{||}^{(1)} \tag{9}$$

After building the interface model, we calculated the ideal work of separation, W_{sep}, to describe the strength of the interface bonding. It is the reversible work that would be needed to separate the

interface into two free surfaces if the plastic and diffusional degrees of freedom were suppressed. With the slab geometry, W_{sep} can be calculated as

$$W_{sep} = (E_{slab1} + E_{slab2} - E_{int})/A \quad (10)$$

where E_{int} is the total energy of the supercell with the interface system; E_{slab1} and E_{slab2} are the total energies of separated slabs calculated when one of the slabs is kept while the other one is replaced by vacuum, A is the interfacial area.

3. Results and Discussion

3.1. Elements Selection

We began our scheme by selection of elements. We calculated electrical resistivity and Pilling–Bedworth ratio of all elementary substance on periodic table and the result is shown in Figure 4. Pilling–Bedworth ratio between 1 and 2 indicates better anticorrosion capacity [21] and smaller electrical resistivity stands for better electrical conductivity. So the green colored circle is our target candidate's zone. Thirteen elements (Cu, Nb, Ni, Hf, Zr, V, Cr, Ti, Mo, Ta, W, Al, and Co) were chosen from target zone with also taking cost into consideration. The distribution of elements shows that elements in the same area on periodic table tend to gather in the same region in Figure 4. IA and IIA elements are located in the yellow zone of Pilling–Bedworth ratio less than 1 with relatively small electrical resistivity, which means bad anticorrosion capacity and good electrical conductivity. Lanthanide and Actinide elements are in the blue circle of Pilling–Worth ratio slightly larger than 1 and electrical resistivity within 5×10^{-7} Ω·m to 1×10^{-6} Ω·m. Most of the transition metals are included in our target zone which matches with the fact that current researches in surface modification for PEMFC bipolar plates mainly focus on transition metals and their compounds.

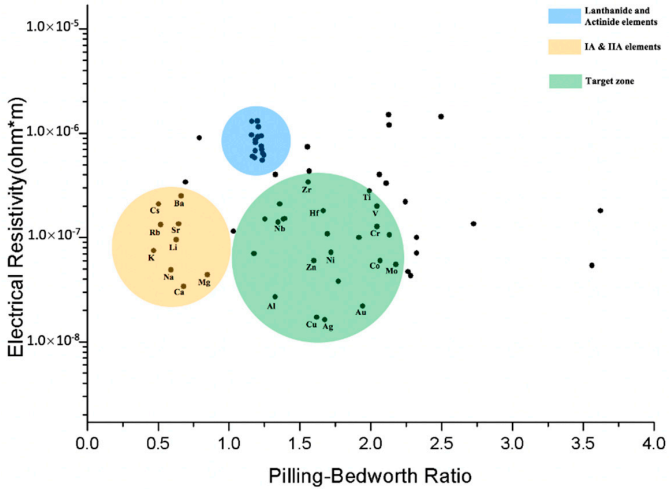

Figure 4. Elements selection through calculation of electrical resistivity and Pilling–Bedworth ratio.

3.2. Electrical Conductivity

The chosen elements were combined with each other to form binary compounds. The corrosion resistance of those stable compounds (energy above hull = 0) were assessed using the Pourbaix approach introduced above. Binary compounds with considerable corrosion resistance were then sent to the computational cluster to calculate their electrical conductivity (σ/τ); results shown in Figure 5, the top ten compounds are displayed. Values of electrical conductivity are at the same order of magnitude with the results of other theoretical studies [28,37]. The result shows carbides and nitrides of transition metal are well conductive and corrosion resistant, which agrees well with the reported experimental results [2,3,11]. Apart from these carbides and nitrides, Ti-composed intermetallic

compounds are also on the list, which is intuitive. Pure titanium and titanium-containing alloys are reported to have high corrosion resistance due to the thin and chemically stable titanium oxide formed naturally on the surface [38,39]. Therefore they are widely applied in chemical processing, biomaterial, and petrochemical industries.

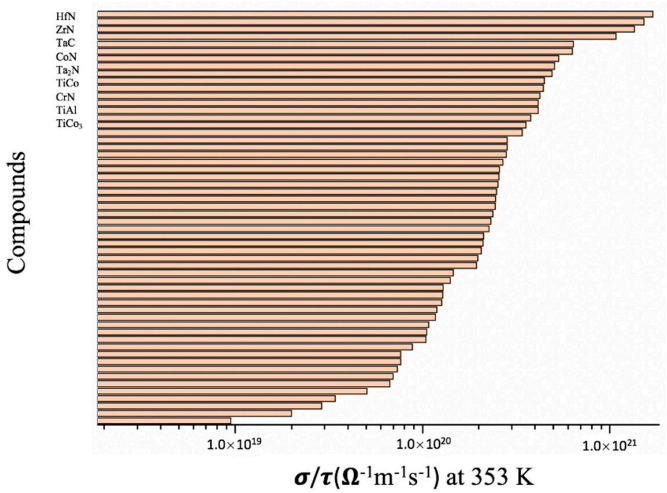

Figure 5. Electrical conductivity of candidate compounds after anticorrosion assessment.

3.3. Separation Work

After corrosion resistance assessment by the Pourbaix diagram approach and electrical conductivity calculation, separation of compounds-stainless steel interfaces was calculated and the results presented in Table 1 in sequence of σ/τ (electrical conductivity) for the top ten compounds. As the results suggest, TiCo and $TiCo_3$, two intermetallic compounds formed between titanium and cobalt, exhibit strong binding with stainless steel substrate. The two compounds are particularly interesting because there is relatively few works about surface modification on PEMFC bipolar plates using titanium–cobalt compounds; the intermetallic composite of the Ti–Co system has already attracted some interest. Lawley et al. [40] developed high hardness/strength Ti–Co intermetallics utilizing powder metallurgy following heat treatment. Martinez-Sanchez et al. [41] synthesized Ti–Co intermetallics by plasma-assisted sintering and mechanical alloying. These works mainly focused on the mechanical properties of Ti–Co intermetallics with little discussion about corrosion resistance and other properties required by bipolar plates. A recent research conducted by Fatoba et al. [42] may act as supporting evidence for the accuracy of our design scheme. They synthesized Ti–Co coatings on a Ti-6Al-4V alloy using the laser metal deposition method and the results showed that the Ti–Co coatings had successfully enhanced the corrosion resistance of the substrate. To study these coating materials in more detail, we suggest that further computational analysis, experimental synthesis, and testing should be carried out.

Table 1. Calculated electrical conductivity and separation work after anticorrosion screening.

Compounds	Common *a* (Å)	$E_{Slab-Fe}$ (eV)	$E_{Slab-com}$ (eV)	E_{Int} (eV)	σ/τ 10^{20} (Ω·ms)$^{-1}$	W_{sep} (J/m^2)
HfN	3.12	−30.61	−85.19	−118.21	17.1	3.9
ZrN	3.15	−30.48	−78.99	−111.74	15.3	3.6
TaC	3.10	−30.67	−86.95	−120.13	13.6	4.2
CoN	2.92	−30.16	−95.32	−125.59	10.8	0.2
Ta_2N	2.98	−30.61	−74.57	−114.43	6.41	16.7
NbN	3.06	−30.34	−88.94	−119.51	6.33	0.4
TiCo	2.85	−30.81	−98.65	−133.74	5.35	8.4
CrN	3.02	−30.48	−97.99	−132.84	5.09	7.6
TiAl	2.85	−30.82	−85.45	−117.02	4.93	1.5
$TiCo_3$	3.23	−30.54	−70.54	−114.41	4.48	20.5

4. Conclusions

A systematic and feasible coating materials design method for PEMFC bipolar plates was established to discover potential candidates using DFT as a tool. Several metrics and criteria were introduced to assess corrosion resistance, electrical conductivity, and binding strength with substrates of hundreds of thousands of materials. The screening scheme is divided into four steps: Elements selection, corrosion resistance assessment, electrical conductivity calculation, and separation work calculation. The results of elements selection shows that elements on the same area of the periodic table tend to gather in the same region on the Pilling–Bedworth ratio electrical resistivity figure. Thirteen elements (Cu, Nb, Ni, Hf, Zr, V, Cr, Ti, Mo, Ta, W, Al, and Co) were chosen from the target zone. The top ten compounds were chosen after Pourbaix diagram-based corrosion resistance assessment and calculation of σ/τ, including HfN, ZrN, TaC, CoN, Ta_2N, TiCo, CrN, TiAl, and $TiCo_3$. After the separation work calculation, TiCo and $TiCo_3$ were recommended as the ultimate candidates because of strong binding with stainless steel. We suggest further computational analysis, experimental synthesis, and testing be conducted to study the two coatings in more detail. This application of computational methods to coating materials design is a step toward more efficient PEMFC bipolar plates development.

Author Contributions: Conceptualization, K.F. and H.Z.; Methodology, K.F.; Software, K.L.; Formal Analysis, L.Y. and Z.L.; Investigation, L.L.; Resources, P.K.C.; Writing—Original Draft Preparation, L.L.; Writing—Review and Editing, K.F.; Visualization, L.Y.; Supervision, K.F.

Funding: This research received no external funding.

Acknowledgments: The authors wish to thank SAIC for financial and technical support, and the University of Michigan and Shanghai Jiao Tong University Joint Institute for helpful discussions. The computations were made possible by the high performance computing system, PI, at Shanghai Jiao Tong University.

Conflicts of Interest: The authors declare no conflict of interest.

References

1. Hinds, G.; Brightman, E. Towards more representative test methods for corrosion resistance of PEMFC metallic bipolar plates. *Int. J. Hydrogen Energy* **2015**, *40*, 2785–2791. [CrossRef]
2. Fetohi, A.E.; Hameed, R.A.; El-Khatib, K.M. Ni–P and Ni–Mo–P modified aluminium alloy 6061 as bipolar plate material for proton exchange membrane fuel cells. *J. Power Sources* **2013**, *240*, 589–597. [CrossRef]
3. Alishahi, M.; Mahboubi, F.; Khoie, S.M.; Aparicio, M.; Hübner, R.; Soldera, F.; Gago, R. Electrochemical behavior of nanocrystalline Ta/TaN multilayer on 316L stainless steel: Novel bipolar plates for proton exchange membrane fuel-cells. *J. Power Sources* **2016**, *322*, 1–9. [CrossRef]
4. Feng, K.; Li, Z.; Sun, H.; Yu, L.; Cai, X.; Wu, Y.; Chu, P.K. C/CrN multilayer coating for polymer electrolyte membrane fuel cell metallic bipolar plates. *J. Power Sources* **2013**, *222*, 351–358. [CrossRef]
5. Bar-On, I.; Kirchain, R.; Roth, R. Technical cost analysis for PEM fuel cells. *J. Power Sources* **2002**, *109*, 71–75. [CrossRef]
6. Mehta, V.; Cooper, J.S. Review and analysis of PEM fuel cell design and manufacturing. *J. Power Sources* **2003**, *114*, 32–53. [CrossRef]
7. Yi, P.; Peng, L.; Zhou, T.; Wu, H.; Lai, X. Cr–N–C multilayer film on 316L stainless steel as bipolar plates for proton exchange membrane fuel cells using closed field unbalanced magnetron sputter ion plating. *Int. J. Hydrogen Energy* **2013**, *38*, 1535–1543. [CrossRef]
8. De Oliveira, M.C.L.; Sayeg, I.J.; Ett, G.; Antunes, R.A. Corrosion behavior of polyphenylene sulfide–carbon black–graphite composites for bipolar plates of polymer electrolyte membrane fuel cells. *Int. J. Hydrogen Energy* **2014**, *39*, 16405–16418. [CrossRef]
9. De Las Heras, N.; Roberts, E.P.L.; Langton, R.; Hodgson, D.R. A review of metal separator plate materials suitable for automotive PEM fuel cells. *Energy Environ. Sci.* **2009**, *2*, 206–214. [CrossRef]
10. Wang, S.; Hou, M.; Zhao, Q.; Jiang, Y.; Wang, Z.; Li, H.; Fu, Y.; Shao, Z. Ti/(Ti, Cr) N/CrN multilayer coated 316L stainless steel by arc ion plating as bipolar plates for proton exchange membrane fuel cells. *J. Energy Chem.* **2017**, *26*, 168–174. [CrossRef]

11. Zhang, H.; Lin, G.; Hou, M.; Hu, L.; Han, Z.; Fu, Y.; Shao, G.S.; Yi, B. CrN/Cr multilayer coating on 316L stainless steel as bipolar plates for proton exchange membrane fuel cells. *J. Power Sources* **2012**, *198*, 176–181. [CrossRef]
12. Yu, H.; Yang, L.; Zhu, L.; Jian, X.; Wang, Z.; Jiang, L. Anticorrosion properties of Ta-coated 316L stainless steel as bipolar plate material in proton exchange membrane fuel cells. *J. Power Sources* **2009**, *191*, 495–500. [CrossRef]
13. Nordin, M.; Herranen, M.; Hogmark, S. Influence of lamellae thickness on the corrosion behaviour of multilayered PVD TiN/CrN coatings. *Thin Solid Films* **1999**, *348*, 202–209. [CrossRef]
14. Chandra, R.; Chawla, A.K.; Kaur, D.; Ayyub, P. Structural, optical and electronic properties of nanocrystalline TiN films. *Nanotechnology* **2005**, *16*, 3053. [CrossRef]
15. Holdren, J.P. *Materials Genome Initiative for Global Competitiveness*; National Science and Technology Council OSTP: Washington, DC, USA, 2011.
16. Greeley, J.; Jaramillo, T.F.; Bonde, J.; Chorkendorff, I.B.; Nã¸Rskov, J.K. Computational high-throughput screening of electrocatalytic materials for hydrogen evolution. *Nat. Mater.* **2006**, *5*, 909–913. [CrossRef] [PubMed]
17. Kirklin, S.; Meredig, B.; Wolverton, C. High-Throughput computational screening of new Li-ion battery anode materials. *Adv. Energy Mater.* **2013**, *3*, 252–262. [CrossRef]
18. Toher, C.; Plata, J.J.; Levy, O.; de Jong, M.; Asta, M.; Nardelli, M.B.; Curtarolo, S. High-throughput computational screening of thermal conductivity, Debye temperature and Grüneisen parameter using a quasi-harmonic Debye Model. *Phys. Rev. B* **2014**, *90*, 174107. [CrossRef]
19. Okimoto, N.; Futatsugi, N.; Fuji, H.; Suenaga, A.; Morimoto, G.; Yanai, R.; Ohno, Y.; Narumi, T.; Taiji, M. High-performance drug discovery: Computational screening by combining docking and molecular dynamics simulations. *PLoS Comput. Biol.* **2009**, *5*, e1000528. [CrossRef] [PubMed]
20. Tong, M.; Lan, Y.; Yang, Q.; Zhong, C. High-throughput computational screening and design of nanoporous materials for methane storage and carbon dioxide capture. *Green Energy Environ.* **2018**, *3*, 107–119. [CrossRef]
21. Xu, C.; Gao, W. Pilling-Bedworth ratio for oxidation of alloys. *Mater. Res. Innov.* **2000**, *3*, 231–235. [CrossRef]
22. Jain, A.; Ong, S.P.; Hautier, G.; Chen, W.; Richards, W.D.; Dacek, S.; Gholia, S.; Gunter, D.; Skinner, D.; Ceder, G.; et al. Commentary: The Materials Project: A materials genome approach to accelerating materials innovation. *APL Mater.* **2013**, *1*, 011002. [CrossRef]
23. Pourbaix, D.; O'KEEKE, T.J. *Encyclopedia of Materials: Science and Technology*; Elsevier: Amsterdam, The Netherlands, 2001; Volume 3, pp. 7774–7781.
24. Ding, R.; Shang, J.X.; Wang, F.H.; Chen, Y. Electrochemical Pourbaix diagrams of Ni Ti alloys from first-principles calculations and experimental aqueous states. *Comput. Mater. Sci.* **2018**, *143*, 431–438. [CrossRef]
25. Schweitzer, G.K.; Pesterfield, L.L. *The Aqueous Chemistry of the Elements*; Oxford University Press: New York, NY, USA, 2010.
26. Persson, K.A.; Waldwick, B.; Lazic, P.; Ceder, G. Prediction of solid-aqueous equilibria: Scheme to combine first-principles calculations of solids with experimental aqueous states. *Phys. Rev. B* **2012**, *85*, 235–438. [CrossRef]
27. Singh, A.K.; Zhou, L.; Shinde, A.; Suram, S.K.; Montoya, J.H.; Winston, D.; Gregoire, J.M.; Persson, K.A. Electrochemical stability of metastable materials. *Chem. Mater.* **2017**, *29*, 10159–10167. [CrossRef]
28. Madsen, G.K.; Singh, D.J. BoltzTraP. A code for calculating band-structure dependent quantities. *Comput. Phys. Commun.* **2006**, *175*, 67–71. [CrossRef]
29. Ahmad, S.; Ahmad, R.; Bilal, M.; Rehman, N.U. DFT studies of thermoelectric properties of R–Au intermetallics at 300 K. *J. Rare Earths* **2018**, *36*, 197–202. [CrossRef]
30. Lee, S.C. Robust mechanical stability, electronic structure, magnetism and thermoelectric properties of CoFeMnSb quaternary Heusler alloy: A first principle study. *J. Alloys Compd.* **2018**, *742*, 903–909.
31. Reshak, A.H. Electronic structure and transport properties of $Ba_2Cd_2Pn_3$ (*Pn* = As and Sb): An efficient materials for energy conversion. *J. Alloys Compd.* **2016**, *670*, 1–11. [CrossRef]
32. Perdew, J.P.; Burke, K.; Ernzerhof, M. Generalized gradient approximation made simple. *Phys. Rev. Lett.* **1996**, *77*, 3865–3868. [CrossRef] [PubMed]
33. Blöchl, P.E.; Jepsen, O.; Andersen, O.K. Improved tetrahedron method for Brillouin-zone integrations. *Phys. Rev. B* **1994**, *49*, 16223. [CrossRef]

34. Kresse, G.; Furthmüller, J. Efficient iterative schemes for ab initio total-energy calculations using a plane-wave basis set. *Phys. Rev. B* **1996**, *54*, 11169. [CrossRef]
35. Fors, D.H.; Johansson, S.A.; Petisme, M.V.; Wahnström, G. Theoretical investigation of moderate misfit and interface energetics in the Fe/VN system. *Comput. Mater. Sci.* **2010**, *50*, 550–559. [CrossRef]
36. Fors, D.H.; Wahnström, G. Theoretical study of interface structure and energetics in semicoherent Fe(001)/*MX*(001) systems (*M* = Sc, Ti, V, Cr, Zr, Nb, Hf, Ta; *X* = C or N). *Phys. Rev. B* **2010**, *82*, 1616–1622. [CrossRef]
37. Choi, G.; Kim, H.S.; Lee, K.; Park, S.H.; Cha, J.; Chung, I.; Lee, W.B. Study on thermal conductivity and electrical resistivity of Al-Cu alloys obtained by Boltzmann transport equation and first-principles simulation: Semi-empirical approach. *J. Alloys Compd.* **2017**, *727*, 1237–1242. [CrossRef]
38. Gowtham, S.; Arunnellaiappan, T.; Rameshbabu, N. An investigation on pulsed DC plasma electrolytic oxidation of cp-Ti and its corrosion behaviour in simulated body fluid. *Surf. Coat. Technol.* **2016**, *301*, 63–73.
39. Dai, N.; Zhang, L.C.; Zhang, J.; Chen, Q.; Wu, M. Corrosion behavior of selective laser melted Ti-6Al-4V alloy in NaCl solution. *Corros. Sci.* **2016**, *102*, 484–489. [CrossRef]
40. Lawley, A.; Gotman, I.; Gutmanas, E.Y.; Koczak, M.J. Design and Processing of Alloys and Composites from Ultrafine Powders. *Adv. Powder Metall. Part. Mater.* **1993**, *6*, 135.
41. Martinez-Sanchez, R.; Gabanas-Moreno, J.G.; Calderon, H.A.; Umemoto, M. Co-Ti Intermetallics Made by Mechanical Alloying. *Mater. Sci. Forum* **1996**, *225–227*, 435–440.
42. Fatoba, O.S.; Adesina, O.S.; Popoola, A.P.I. Evaluation of microstructure, microhardness, and electrochemical properties of laser-deposited Ti-Co coatings on Ti-6Al-4V Alloy. *Int. J. Adv. Manuf. Technol.* **2018**, *97*, 2341–2350. [CrossRef]